The Meteoritical Society

Meteoritics & Planetary Science 56, Nr 11, 1988–2001 (2021)
doi: 10.1111/maps.13759

^{3}He flux obtained from South Pole air and snow-ice and its connection to interplanetary dust particles

Kenneth A. FARLEY[1], Susan TAYLOR[2*†], Jonathan TREFFKORN[1], James H. LEVER[2], and Anthony L. GOW[2†]

[1]California Institute of Technology, Pasadena, California 91125, USA
[2]US Army Engineer Research and Development Center Cold Regions Research and Engineering Laboratory, Hanover, New Hampshire 03755, USA
*Corresponding author. E-mail: susant47@gmail.com

(Received 27 May 2021; revision accepted 02 October 2021)

Abstract–Researchers have characterized extraterrestrial (ET) helium, likely carried by interplanetary dust particles (IDPs), in deep-sea sediments spanning more than the last 100 Myr. Here we complement those low resolution and deep time studies by measuring He in modern Antarctic air and recent ice. We analyzed 180 air filter samples collected in 2017 and 2018 at the South Pole and detected ^{3}He above blank levels in 178. The filters collected during the austral springs had elevated ^{3}He in multiple subsamples indicating the presence of many individual IDPs and potentially, a temporal variation in the ET small particle flux. Our calculated mean ^{3}He flux of $1.4 \pm 1.2 \times 10^{-12}$ cc STP cm^{-2} ka^{-1} is the first such measurement from air samples. We also melted, filtered, and analyzed one hundred and forty-one 1 m-long ice sections from a ~2000-yr-old South Pole core. We detected ^{3}He above blank levels in 139 of the 141 ice core samples and calculated an average flux of $1.2 \pm 0.3 \times 10^{-12}$ cc STP cm^{-2} ka^{-1}. Our two flux values are within a factor of two of those calculated from stratospheric IDP concentrations, those previously measured for sections of the GISP2 and Vostok ice cores, and from sediment cores from different locations and ages. The similarity of these flux values over disparate time scales (1–10^8 yr) and geographic locations (90° S to equator) indicates modest temporal variability and remarkable agreement among diverse IDP archives. These data provide a compelling link from IDPs collected in the stratosphere to those recorded in deep time sedimentary archives.

INTRODUCTION

Cosmic dust is the umbrella term for small extraterrestrial (ET) particles arriving on the Earth and comprises interplanetary dust particles (IDPs), generally <20 μm in size, and micrometeorites (MMs), generally <2 mm in size. MMs account for most of the ET mass deposited on present-day Earth (Love & Brownlee, 1993), and although IDPs add little ET mass they are of great interest to planetary scientists. Many are not small rocks but fragile agglomerations of grains, primitive materials that shed light on the nature of matter when our solar system formed. Evidence of their primitive nature includes their porous, fragile, fine-grained structures (Bradley et al., 1983); highly unequilibrated chemistries and anhydrous mineralogy; high concentrations of presolar grains (Messenger et al., 2003); the presence of glass with embedded metal and sulfides (Bradley, 1994); abundant organic matter (Thomas et al., 1993); and H, C, or N isotopic anomalies in the organics (Messenger, 2000).

Using high-flying aircraft, NASA began collecting IDPs in the stratosphere in 1981. Most flights are carried out on an opportunity basis but some stratospheric flights have been timed to collect particles from specific comet dust streams, e.g., 26P/Grigg-Skjellerup (Busemann et al., 2009; Messenger, 2002) and comet 21P/Giacobini-Zinner (Nakamura-Messenger et al., 2015). More recently, samples from melted Antarctic snow show that highly primitive materials can

[†]Retired

be collected on the Earth's surface (Noguchi et al., 2015), including particles with affinities to Wild 2 comet grains, and rare ultracarbonaceous particles (Dobrica et al., 2009; Duprat et al., 2010). Their presence in Antarctic snow and ice suggests that IDPs must also be present in the near-surface air (Taylor et al., 2016). To collect IDPs, Taylor et al. (2020) filtered the extremely clean air at the South Pole station from November 2016 to January 2019.

Helium-3 is a stable nuclide that is present in very high concentrations in IDPs but not in most MMs (Baecker et al., 2018) or in terrestrial materials. Because IDPs are small and have high surface-to-volume ratios, solar wind ions are implanted in or on IDP surfaces, while the IDPs are in space. During atmospheric entry, a fraction of the smallest of the ET grains (<10 μm) may enter at temperatures below about 600 °C and therefore retain their burden of solar wind helium (Farley et al., 1997). This is generally not the case for the larger MMs (Taylor et al., 2000). Over 80% of MMs melt transiting the Earth's atmosphere and many of the remainder are highly heated (Taylor et al., 2012). As solar wind ^{3}He/^{4}He ratios are far higher than terrestrial ones, ^{3}He can be used as a tracer of IDPs.

NASA's stratospheric flights collected IDPs on clean "flags," and from the volume of air swept by each flag, have resulted in two estimates of IDP numerical concentrations per m^3 of air: 1.2×10^{-3} (Brownlee et al., 1977) and 2.5×10^{-3} (Zolensky and Mackinnon, 1985). Pepin et al. (2000) measured the ^{3}He concentration in individual stratospheric IDPs and found a median value of 1×10^{-5} cc STP g^{-1} per IDP with a range in ^{3}He concentration of almost a factor of 100. Nier and Schlutter (1992) measured helium step-heating release patterns of IDPs and inferred a cometary or asteroidal origin based on ^{3}He's release pattern and maximum release temperature.

Melted ice core samples have been measured for ^{3}He. Brook et al. (2000) measured ice deposited 400–430 yr ago from the Greenland GISP2 core, and two sections of the Antarctic Vostok core, one deposited 3.80 ka ago and 17 samples from sections of core deposited between 75 and 97 ka before present. Ice cores have the advantage, relative to deep-sea sediments, of being very well dated but the disadvantage of low IDP numbers, necessitating large sample sizes to reduce statistical imprecision. Brook et al. (2000) calculated an average ^{3}He flux of $0.62 \pm 0.27 \times 10^{-12}$ cc STP cm^{-2} ka^{-1} for the GISP core section and a flux of $0.77 \pm 0.25 \times 10^{-12}$ cc STP cm^{-2} ka^{-1} for the 3.80 ka Vostok section. Using data published by Brook et al. (2000), we calculated an average flux of $0.94 \pm 0.6 \times 10^{-12}$ cc STP cm^{-2} ka^{-1} for the 75–97 ka Vostok sections but omitted two values from the average because they were much higher than the rest. Such high values suggest analysis of rare large or He-rich particles (Farley et al., 1997).

Helium-3 (and other geochemical tracers) has also been measured in seafloor sediments as a way to document changes in the interplanetary dust flux through time (given known sedimentation rates) or to constrain sedimentation rates (knowing ET flux). The million-year average for the ^{3}He measured from a variety of sediment cores from different locations is about 1×10^{-12} cm^3 STP cm^{-2} kyr (Farley & Patterson, 1995; Marcantonio et al., 1996, 1998, 1999; Patterson & Farley, 1998). Farley et al. (1997) discussed how the mass and particle size of the ^{3}He-bearing phase is information that is needed to assess sedimentary redistribution and the variability in He abundances in both sediment and ice cores.

The objectives of this work were to (1) measure the IDP flux in terrestrial surface air and in near-surface (200 m) ice core samples, (2) provide the link between the IDP flux measured in the stratosphere and ^{3}He flux measurements made on deep ice cores and on deep-sea sediments, and (3) look for evidence of temporal variations in the IDP flux on monthly (air samples) and decadal (ice core) time scales. To accomplish our goals, we subsampled and analyzed 13 of the 41 air filters collected at the South Pole for ^{3}He, 7 collected in 2017 and 6 in 2018 (Taylor et al., 2020). We also melted and filtered a 201 m core drilled at the South Pole in 1981 (Kuivinen et al., 1982).

MATERIALS AND METHODS

Air Filter Samples

Air filter samples were obtained from a NASA-funded experiment to collect IDPs (Taylor et al., 2020). Air from the clean-air sector at the Amundsen Scott South Pole station was drawn into a 20 cm diameter aluminum pipe and through a polycarbonate membrane filter etched with 3 μm pores at a density of 2×10^6 pores cm^{-2} (Appendix A). The air was suctioned at ~6 m s^{-1} or about 400,000 m^3 per month. The experiment ran almost continuously between the end of November 2016 and the beginning of January 2019.

We analyzed ^{3}He abundances in 13 of the 41 filters collected, 7 from 2017 and 6 from 2018. One cm^2 subsections were cut with stainless steel scissors, from filter strips generally located edge to edge across the widest part of the filter (Fig. 1). Each filter had an area of ~300 cm^2, so 20 subsamples, each 1 cm^2 in area, represent about 5% of the total filter area. We assume

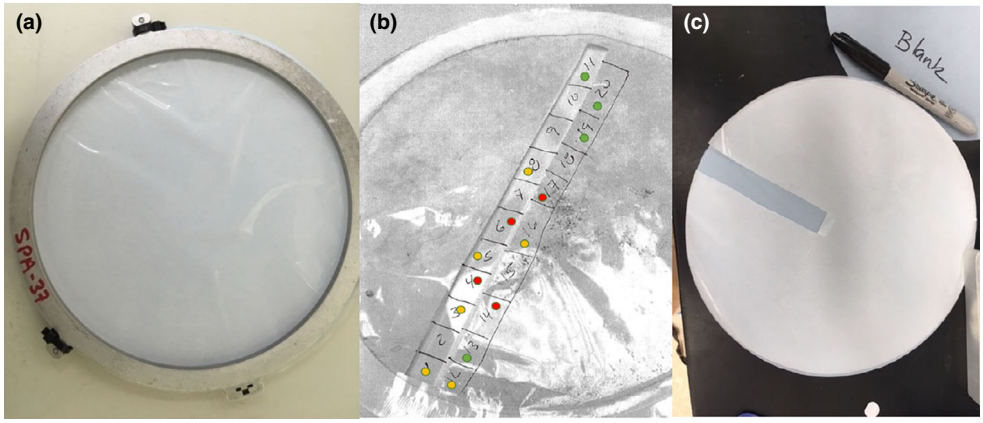

Fig. 1. Images showing (a) uncut filter, (b) cut filter showing location of sequentially numbered ~1 cm^2 samples color-coded with red having the most ^{3}He, and (c) section analyzed in unexposed "blank" filter. (Color figure can be viewed at wileyonlinelibrary.com.)

uniform airflow across the filter and calculate the volume of air suctioned through each filter via measured flow velocities and exposure times.

Ice Core Samples

A 201 m deep core was electro-mechanically drilled at the South Pole during the 1981–1982 Antarctic season (Kuivinen et al., 1982—the stratigraphy of the core is shown in Appendix B). The core was 96–99 mm (3.8–3.9 inches) in diameter and spanned 2026 yr (45 BC–1981 AD). It was collected and stored as meter-long sections, each sampling about 10 yr of snow deposition (10.2 ± 2.2). Its age–depth relationship is not quite linear because porosity reduces with depth; no lateral shearing of the ice was observed. Surface snow layers are thicker (15 cm or 6 yr per m of core) than the ice layers near the base (8.8 cm or 11.4 yr per m of core; Hogan & Gow, 1997). Half of the core was used to determine its geochemical properties (Mosley-Thompson & Thompson, 1983; Stauffer & Schwander, 1983). The other half was shipped to the Cold Regions Research and Engineering Laboratory (CRREL) in Hanover, New Hampshire, and stored at −20 °C.

In 2018, we passively melted the remaining half of the core (185 of the 201 sections, each 1 m in length) in a clean room at CRREL. Each core section was placed in a plexiglass tube atop a stainless steel funnel, the stem of which held a 47 mm diameter Whatman glass filter (Fig. 2). A single filter was used for each meter of core yielding 185 samples, of which 141 were analyzed. The temperature in the lab was 22 °C and each core took about 20 h to melt.

We noticed that the cores had a faint petroleum-like smell. As the core was drilled near the airfield taxiway (Kuivinen et al., 1982), we think the smell is likely hydrocarbons from the plane exhaust that could have contaminated the cores while they were being collected and examined in 1981. While melting the cores, we also noticed an oily residue building up on the inside of the stainless steel funnel. About 50 of the cores had been melted when we first wiped the inside of the funnel with a Whatman glass filter. We wiped the funnel two more times over the course of melting and once at the end. These samples were also analyzed for ^{3}He.

Helium Analytical Methods

Helium-3 analyses were conducted at Caltech. The 1 cm^2 polycarbonate filter subsamples and the dry 47 mm diameter glass filters used for each core sample were placed in tin cups and compressed to form a compact ball. The samples were treated similar to seafloor sediments for ^{3}He extraction (Patterson & Farley, 1998) with the notable addition of a liquid nitrogen U-trap described below. The tin foil balls were loaded into an ultrahigh vacuum autosampler that allows sequential introduction of the balls into a resistance furnace. The vacuum furnace and samples were pumped down with a turbomolecular pump for at least 30 min before outgassing the furnace for at least 80 min at ~1300 °C directly into the pump.

Prior to sample analysis, hot furnace blanks were analyzed, and when the blank was less than 0.2×10^{-9} cc STP ^{4}He, the samples were analyzed. Samples and blanks, including pieces of unexposed filter, were heated to 1200 °C for 30 min, and then allowed to cool for an additional 15 min. For the duration of sample heating and cooling, the resulting gases were exposed to a charcoal-bearing U-trap at liquid nitrogen temperature to perform an initial

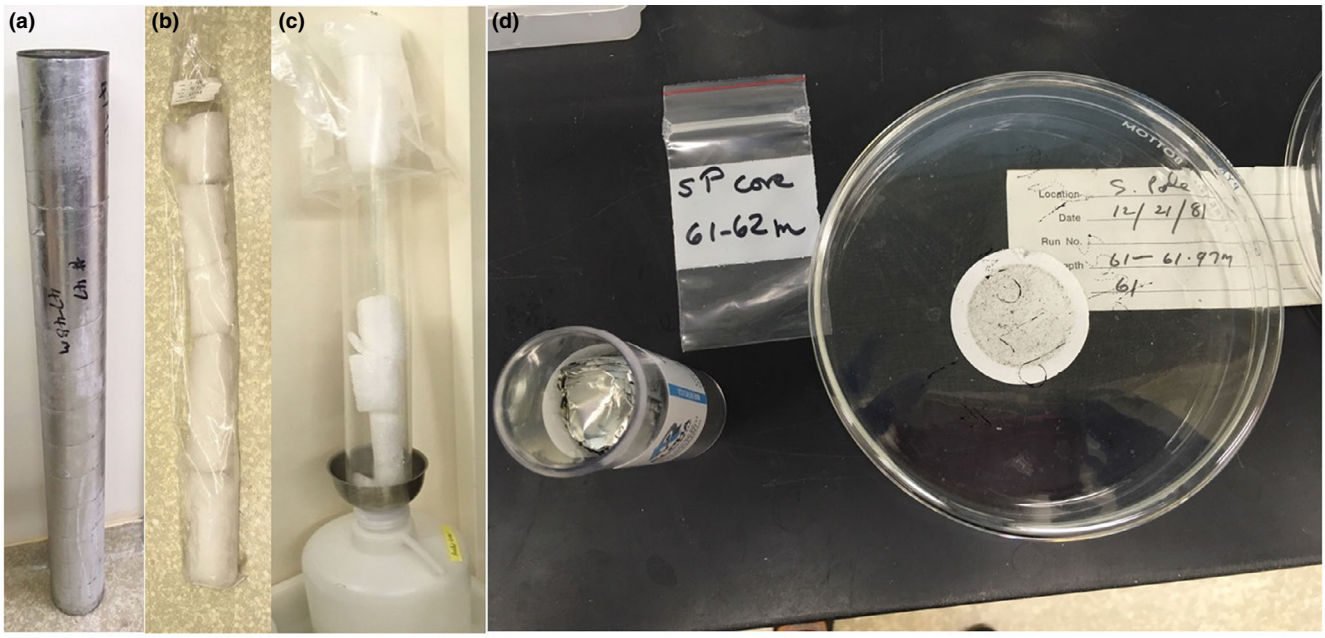

Fig. 2. Labeled cardboard tubes (a) containing bagged and tagged core sections (b) collected at the South Pole in 1981. Each core was removed from its bag and put in an acrylic tube placed on a stainless-steel funnel (c) and melted in a cleanroom at CRREL in 2018. After melting, each filter sample (D) was removed from the funnel, dried, and placed in a tin cup for analyses at Caltech. (Color figure can be viewed at wileyonlinelibrary.com.)

purification of evolved He. In particular, heavier noble gases (Ar-Xe), water, CO_2, and any organic contaminants from the melted polycarbonate filter were trapped at this stage.

After furnace cooling, evolved gases not sorbed on the charcoal (typically He, Ne, H_2, and some CH_4) were introduced into the vacuum purification line. These gases were sequentially exposed to three SAES NP10 getters and a secondary charcoal-bearing liquid nitrogen trap before sorption on charcoal held at 14 K. The cryo-focused and cryo-purified He was released from the charcoal at 34°K, and introduced into a Thermo Helix SFT mass spectrometer. ^{3}He was measured on a pulse counting electron multiplier. ^{4}He was usually measured on both a 10^{11} Ohm Faraday detector in simultaneous detection mode, and the electron multiplier after an electric field hop. In some cases, there was too much ^{4}He to permit electron multiplier measurement of this isotope.

Hot blanks were interspersed between filter analyses. Average ^{3}He and ^{4}He hot blanks were ~1.2×10^{-15} and 0.15×10^{-9} cc STP, respectively. Tin foil used to contain samples contributes no observable helium above this level. Five unexposed sections of a filter were also analyzed as blanks. These samples carried no detectable ^{4}He above blank ($0.15 \pm 0.06 \times 10^{-9}$ cc without hot blank correction), but had noticeably more ^{3}He, averaging $3 \pm 0.4 \times 10^{-15}$ cc cm^{-2}. The filter blank has a ^{3}He/^{4}He higher than the atmospheric ratio. Whether this reflects some unknown and unusual source of helium associated with the manufacture of the nucleopore filter, or accumulation of memory from previous samples within the furnace or vacuum system, is unknown. Regardless, these blanks were subtracted from all reported analyses. While the ^{3}He blank was seldom more than 10% of the sample ^{3}He, in many cases the ^{4}He blank correction was very substantial, and in some cases it was larger than the total amount of ^{4}He measured. When measured ^{4}He was less than 0.21×10^{-9} (equal to the filter blank + 1σ), ^{4}He is reported as not detected (ND). Instrumental fractionation and sensitivity were determined using a manometrically calibrated synthetic standard with a ^{3}He/^{4}He ratio of 2.05 R_A analyzed multiple times during each batch of 12 samples. R_A is the ^{3}He/^{4}He ratio divided by the ^{3}He/^{4}He ratio in air (1.39×10^{-6}).

The above represents a typical helium gas analysis. However, the polycarbonate filters necessitated the addition of a decontamination procedure unique to these analyses. To protect the vacuum purification line from organic contamination, the charcoal U-trap was removed and cleaned between each batch of samples. The trap was removed while still frozen, warmed, and cleaned three times with acetone in an ultrasonic bath.

Table 1. Average ^{3}He concentrations $\pm$ 1σ, average ^{3}He fluxes (cm^2 per month), and other information relating to the filters sampled.

	Filter #	Days exposed	Volume air filtered (m^3)	^{3}He Conc. (ave.) $\times 10^{-12}$ cc STP	^{3}He Flux (ave.) $\times 10^{-12}$ cc STP cm^{-2} mo^{-1}	Filter area cm^2
Spr. 2016	SPA-1	0.25	4004	0.01 $\pm$ 0.02	1.61 $\pm$ 2.5	3
Sum. 2017	SPA-4	35	579,512		0.015	4
				0.016 $\pm$ 0.004	0.014 $\pm$.004	20
Fall 2017	SPA-8	28	539,611	0.02 $\pm$ 0.023	0.021 $\pm$ 0.025	18
	SPA-10	35	817,017	0.044 $\pm$ 0.028	0.038 $\pm$ 0.025	20
Win. 2017	SPA-13	14	288,806	0.02 $\pm$ 0.014	0.044 $\pm$ 0.030	20
Spr. 2017	SPA-17	22	352,322	0.106 $\pm$ 0.141	0.146 $\pm$ 0.195	19
	SPA-22	14	254,605	0.012 $\pm$ 0.028	0.026 $\pm$ 0.061	20
Sum. 2018	SPA-27	14	190,004	0.002 $\pm$ 0.002	0.005 $\pm$ 0.005	9
Fall 2018	SPA-30	38	794,217	0.025 $\pm$ 0.019	0.02 $\pm$ 0.015	10
Spr. 2018	SPA-35	13	278,763	0.038 $\pm$ 0.051	0.089 $\pm$ 0.12	15
	SPA-37	7	123,503	0.003 $\pm$ 0.003	0.013 $\pm$ 0.012	13
	SPA-39	7	110,202	0.004 $\pm$ 0.01	0.017 $\pm$ 0.005	9
Sum. 2019	SPA-45	1	14,929	0	0	2

Before being reattached to the line, the trap was dried at 100 °C and reloaded with new charcoal.

RESULTS AND DISCUSSION

Air Filter ^{3}He

Our goals in analyzing the filters were to measure the ^{3}He flux and assess its heterogeneity and seasonal variation. Statistical heterogeneity is expected given the discrete nature of IDPs and the high ^{3}He concentration of individual IDPs (Farley et al., 1997). The filters selected for analysis were exposed during different seasons of the austral year. Initially, we analyzed ^{3}He from a single 4 cm^2 piece of filter SPA-4 to test if ^{3}He was present. A positive result led us to analyze subsamples of 13 filters, 7 from 2017 and 6 from 2018, for a total of 180 subsamples. Results are summarized in Table 1 and plotted in Figs. 3–7. All data are listed in Appendix C.

We detected ^{3}He above blank levels in 178 of the 180 filter subsamples with amounts ranging from ~2 to ~640 $\times$ 10^{-15} cc STP (Fig. 3). The ^{3}He distribution peaks at about 16 $\times$ 10^{-15} cc STP, with a long but reasonably well-populated tail extending to ~250 $\times$ 10^{-15} cc STP. The SPA-17 subsample at 640 $\times$ 10^{-15} cc STP is far higher than the next highest subsample.

Of the 180 subsamples, 110 also had ^{4}He above the detection limit. In a plot of ^{3}He versus ^{4}He (Fig. 4), the subsamples with ^{4}He lie on or below a line of slope 3.0 $\times$ 10^{-4} defined by the Filter 17 subsamples, very similar to the ratio of fractionated solar wind in stratospheric IDPs (Nier & Schlutter, 2000). Figure 4 breaks out the subsamples by filter number and reveals large heterogeneity both within and among the filters. For example, Filter 17 spans the entire diagram, from subsamples plotting near the origin to the most ^{3}He-rich subsample measured. Filters 8, 10, 22, 30, and 35 have one or more subsamples plotting well up along the solar wind He trendline. The remainder of the subsamples plot in a cluster with low ^{3}He and ^{4}He. We considered whether the variability in ^{3}He observed among filter subsamples was comparable to purely statistical variability. Farley et al. (1997) modeled the variability expected from the accumulation of a small number of IDPs on terrestrial surfaces as a function of area-time product. The smallest area-time product modeled (0.025 m^2 yr) had a spread of about a factor of 4 at the 95% limits of the distribution (Farley et al., 1997). Smaller area-time products for the air samples (~0.003 m^2 yr) should make this range larger. Figure 3 shows about a factor of 8 range among the air filter subsamples at the 95% limits of the distribution. The observed ranges are thus not unreasonable in comparison to the model, though new modeling of this smaller area-time product would strengthen this conclusion.

A few samples have elevated ^{4}He for a given ^{3}He, suggesting the addition of terrestrial helium probably carried by windblown continental mineral grains. Two subsamples from SPA-4, SPA-8, and SPA-10, four from SPA-22, and one from both SPA-13 and SPA-37 have elevated levels of terrestrial ^{4}He (Fig. 4). Filters with multiple subsamples with elevated terrestrial He, however, are unremarkable in their ^{3}He abundance distribution. The unusual SPA-17, with abundant solar-wind like ^{3}He, has no subsamples with measurable terrestrial He, suggesting that the producers of terrestrial He do not affect the ET helium.

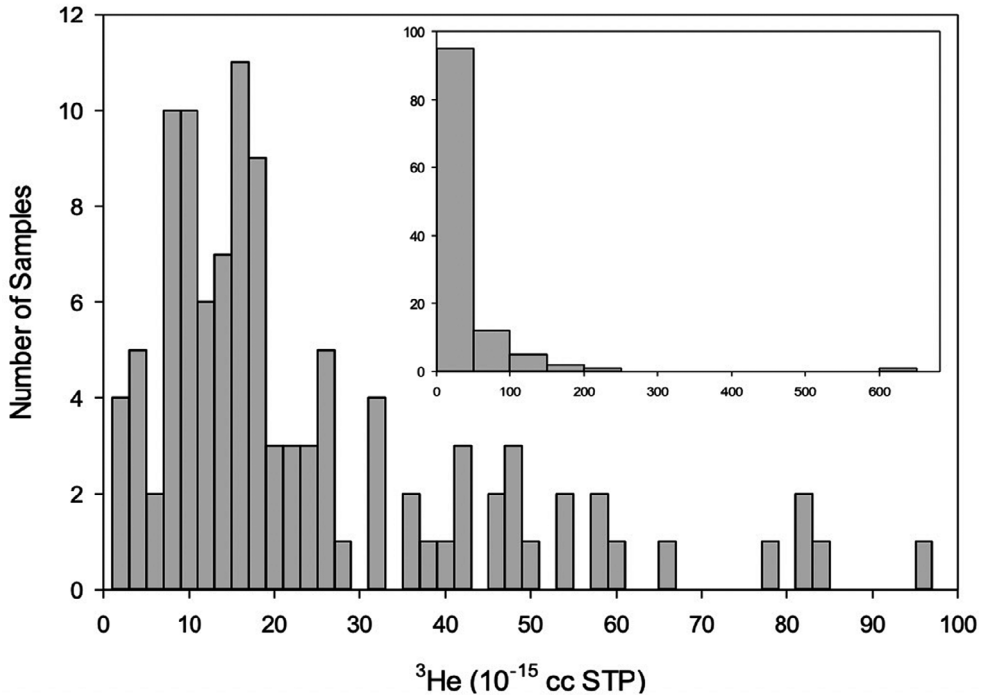

Fig. 3. Blank-corrected ^{3}He abundances in the 178 filter subsamples with He. The 2σ uncertainty in the blank is comparable to the size of one bar in the main plot, confirming that the 178 values plotted had clearly detected ^{3}He.

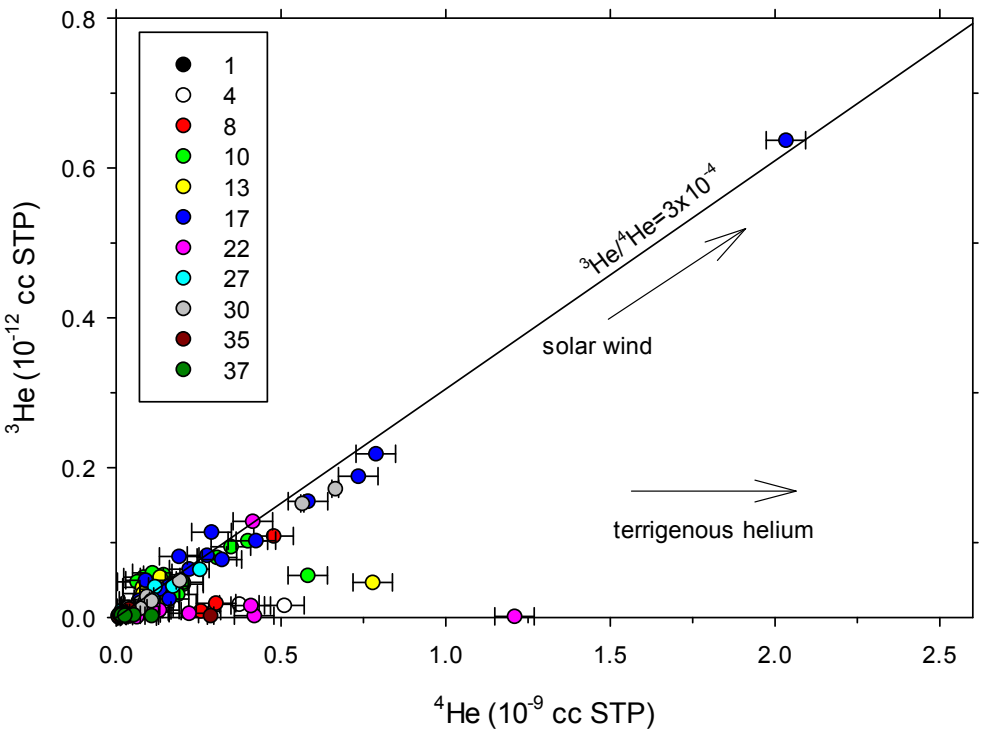

Fig. 4. ^{3}He versus ^{4}He in the 110 subsamples with measurable ^{4}He above blank level. Colors indicate the filter from which each subsample was taken. Line of slope $^3\text{He}/^4\text{He} = 3.0 \times 10^{-4}$ was obtained by linear regression of the SPA-17 subsamples. This ratio is similar to that of the fractionated solar wind in stratospheric IDPs (Nier & Schlutter, 1992), and defines an upper bound for the ^{3}He/^{4}He ratio measured on the filter subsamples.

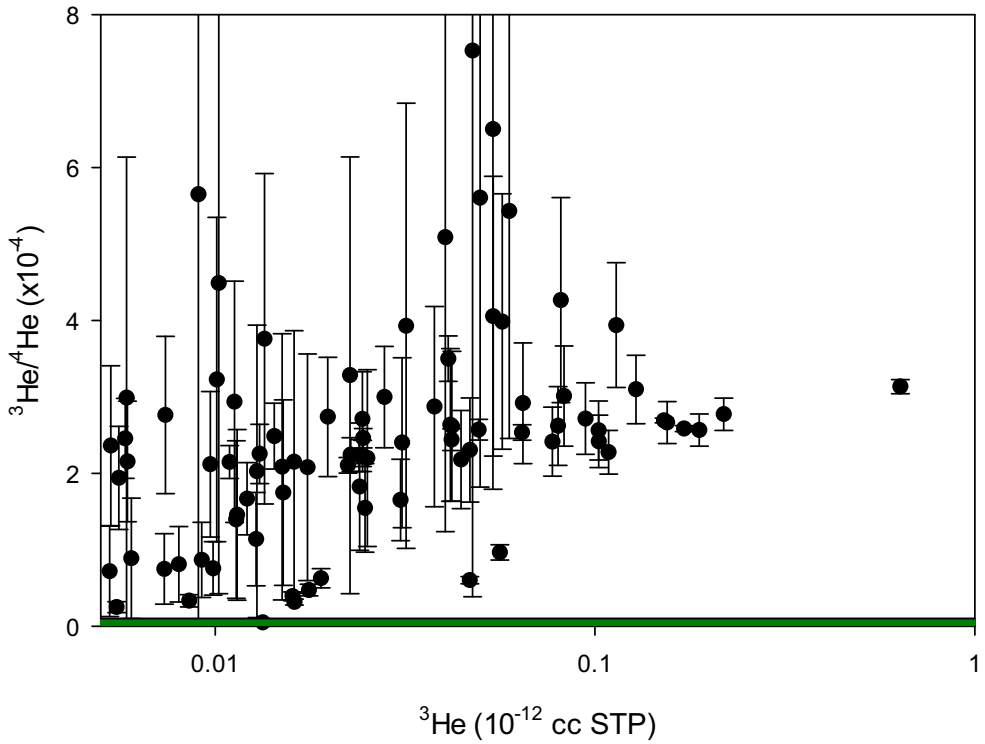

Fig. 5. Blank-corrected ^{3}He/^{4}He ratios versus ^{3}He abundance. While samples with low ^{3}He abundance have lower ^{3}He/^{4}He ratios, those ratios are nevertheless far higher than plausible purely terrigenous sources (bar at base of plot shows the range of terrestrial values, $<1 \times 10^{-5}$ cc STP). This observation suggests that even the low ^{3}He samples carry ET helium. (Color figure can be viewed at wileyonlinelibrary.com.)

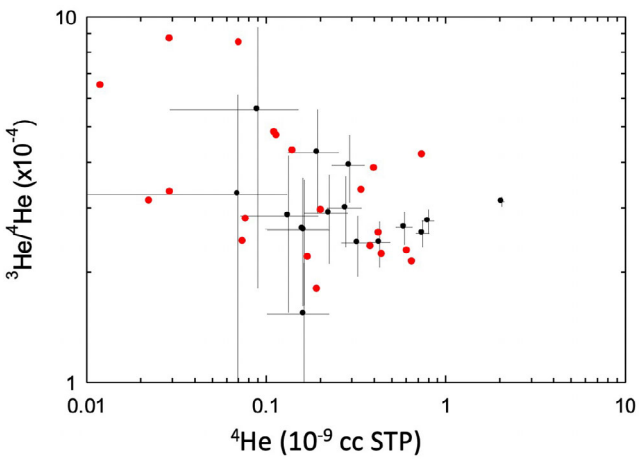

Fig. 6. SPA-17 subsample values (with error bars) compared to individual stratospheric IDP values (no error bars) from Pepin et al. (2000). ^{3}He on the filter subsamples is directly comparable in isotopic composition and concentration to the individual nanogram-size stratospheric particles. (Color figure can be viewed at wileyonlinelibrary.com.)

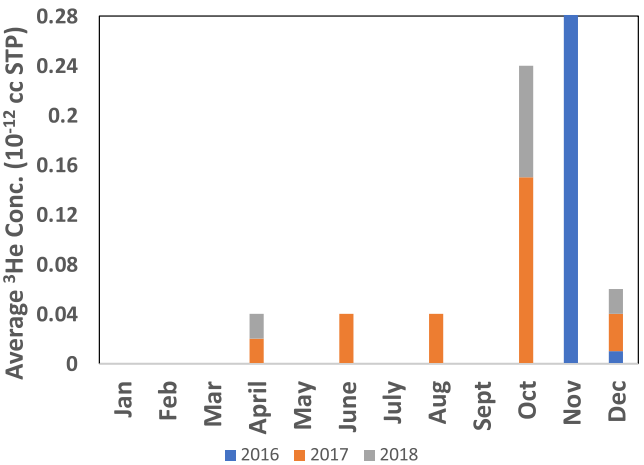

Fig. 7. Average ^{3}He concentrations, normalized for exposure time, plotted per month for 2 yr of collection. No filter pieces were measured for the months showing no concentration. The ^{3}He value for SPA-1 (November 2016) lies well above the range plotted at 1.6×10^{-12}cc STP (Table 1). The standard deviations of the plotted ^{3}He averages are large (Appendix C).

To check whether the subsamples with low He abundance (e.g., those forming the peak in the histogram in Fig. 3 at 8 to 18 $\times$ 10^{-15} cc STP) actually contain ET He or whether purely terrestrial sources could explain the values, we plotted the ^{3}He/^{4}He ratio against the ^{3}He abundance (both blank corrected).

Figure 5 shows that while samples with lower ^{3}He have somewhat lower ^{3}He/^{4}He ratios, the lowest ratios are in the vicinity of 1×10^{-4}. Terrestrial sources generally have much lower ^{3}He/^{4}He ratios. For example, mantle (volcanic) ^{3}He/^{4}He ratios rarely exceed 10^{-5} (Farley & Patterson, 1995). Similarly, while cosmic ray irradiation of surface rocks produces ^{3}He/^{4}He ratios of about 0.1, the rocks themselves inevitably carry radiogenic ^{4}He, and thus much lower ^{3}He/^{4}He ratios. Based on this plot it seems very likely that even the low ^{3}He subsamples carry ET helium, most likely accompanied by a small amount of terrestrial He to account for the reduction in the ^{3}He/^{4}He ratio.

For SPA-17, the distribution of elevated ^{3}He across multiple subsamples is consistent with the presence of many individual IDPs. The ^{3}He concentrations and the ^{3}He/^{4}He ratios measured in SPA-17 subsamples overlap measurements from individual stratospheric particles (Fig. 6), whose masses range from 0.06 to 48 ng (Pepin et al., 2000). This correspondence between individual subsamples and IDPs suggests that filter SPA-17 must have orders of nanograms of ET mass on it.

Temporal Variability in Air Filter ^{3}He Concentrations

The ^{3}He concentrations, normalized by volume of air filtered, are shown in Fig. 7. The measurements made over ~2 yr show that the austral spring has elevated ^{3}He deposition relative to other seasons. SPA-1 (November 30, 2016) has an order of magnitude higher value (1.6×10^{-12}cc STP) than the other samples, followed by SPA-17 (October 16–November 7, 2017) and SPA-35 (October 22–November 4, 2018). The value for SPA-1 is not as certain as those for SPA-17 and 35 because the filter was only exposed for 5 h (4004 m^3) producing a large multiplying factor when normalized. Also, only three subsamples were analyzed (Table 1). Nevertheless, we think this filter likely has high ET levels because an 8 μm IDP was found on a different 1 cm^2 piece of SPA-1 examined by scanning electron microscopy (Taylor et al., 2020). The only other filter exposed for such a short period of time (SPA-45) had no ^{3}He. These measurements suggest that the IDP flux is perhaps 5–10 times higher during the austral spring (October–November) than at other times.

Interestingly, radar measurements (Janches et al., 2004) and chemical analyses of aerosols (Cunningham & Zoller, 1981) at the South Pole show increases in the ET flux during the austral summer and not during spring. Radar measures meteors, particles larger than IDPs, whose rates peak in the summer when Antarctica has a forward-facing orientation relative to the ecliptic (Janches et al., 2004). The aerosol-sized meteoritic component, on the other hand, is submicron and smaller than IDPs. Its seasonality is thought to be linked to the behavior of air movement over Antarctica. During the austral summer, tropospheric air descends over the South Pole, whereas during the winter, a strong inversion isolates the surface air from the tropospheric and stratospheric air (Bodhaine et al., 1986). If IDPs accumulated in the stratosphere, weakening of the inversion in the spring might cause the enrichment we see.

Earth's passage through IDP-rich space (e.g., comet trails associated with meteor streams) might also cause the enrichment. Several candidate meteor showers are active in the Southern hemisphere from July to November: Southern Delta Aquarids (July 12–August 23, radiant −16, 41 km s^{-1}); Alpha Capricornids (July 3–August 15, radiant −10, 23 km s^{-1}); Daytime Sexantids (September 9–October 9, radiant 0, 32 km s^{-1}); and the Southern Taurids (September 10–November 20, radiant +9, 27 km s^{-1}) (Jenniskens et al., 2017; http://cams.seti.org/FDL/, https://en.wikipedia.org/wiki/List_of_meteor_showers). We include showers that peak in July as small particles could take several months to reach the surface (Messenger, 2002) and note that no single shower stands out as a strong candidate. Maybe the IDPs on the filters come from an unknown stream or one whose particles are too small for visual or radar detection. Low-entry-velocity IDPs, trapped in quasi-satellite resonance around the Earth (Kortenkamp, 2013), are one such possibility.

South Pole Core ^{3}He

Our goals for the South Pole core measurements were to obtain a 2000-yr record of ^{3}He surface deposition to compare with the air measurements. We detected ^{3}He above blank levels in 139 of the 141 ice core sections analyzed. The data are shown in Figs. 8 through 11, Table 2, and Appendix D. The South Pole ice cores had an average ^{3}He value of ~0.5×10^{-12} cc STP (Fig. 8), with most ^{3}He values $<2 \times 10^{-12}$ cc STP.

Of the 141 cores measured, 139 also had ^{4}He above the detection limit. In a plot of ^{3}He versus ^{4}He (Fig. 9), the cores with high ^{3}He values lie near the fractionated solar wind helium line of slope 3.0×10^{-4} (Nier & Schlutter, 1992; Pepin et al., 2000) while most plot in a cluster with low ^{3}He and ^{4}He and several have fairly high ^{4}He values. We also plotted some of the air filter data to show that the ranges of the data sets are similar. The higher ^{3}He in the ice cores results from their longer sampling times (the data have not been normalized by time here). The lower ^{3}He/^{4}He ratios of the ice cores are also explained by longer sampling times that allow for more terrestrial ^{4}He to deposit in the ice.

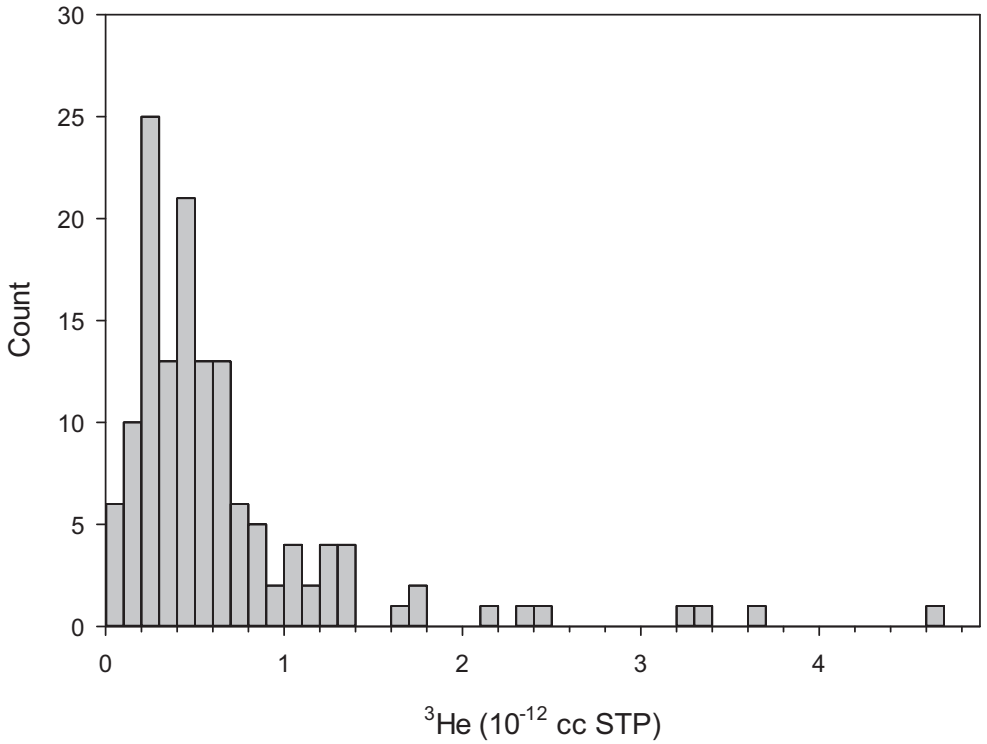

Fig. 8. Histogram showing ^{3}He concentrations in 137 of the 139 ice core sections with measurable ^{3}He. The two cores not plotted had values of 11 and 18.1 $\times$ 10^{-12} cc STP.

Figure 10A plots the ^{3}He concentrations as a function of depth in meters for all of the cores with measurable He. Most of the concentrations are below 2×10^{-12} cc STP with only nine outliers. Values below 2×10^{-12} cc STP are remarkably similar as evidenced by the running average concentration (line in Fig. 10B). This similarity indicates that the flux has been quite constant over the last 2000 yr with most yearly variability averaged out by the 10-yr measurement period.

Figure 10C shows the helium isotope ratios, which were used to deconvolve the ^{3}He into ET and terrestrial components. The average ^{3}He/^{4}He value for these samples is $1.04 \pm 0.71 \times 10^{-4}$. This high value indicates that the ^{3}He is ET in origin since terrestrial sources generally have much lower ^{3}He/^{4}He ratios (Farley & Patterson, 1995). The ratios we measure, however, are about half of those measured for IDPs (2.6 ± 0.25 ^{3}He/^{4}He $\times$ 10^{-4}, measured on 36 IDPs, Nier & Schlutter, 1992) suggesting the addition of terrestrial dust that carries ^{4}He into the ice.

Although we see no obvious temporal pattern in the ^{3}He values in Fig. 10, when we look at the nine cores that have ^{3}He values larger than 2×10^{-12} cc STP, six of them cluster between the years 660 and 1070 AD and have a reoccurrence interval of 102 ± 20 yr (Fig. 10A circled, Table 2). The last interval, ending ~1170 AD (94 m), shows a large increase in ^{3}He as one might expect if a short period comet were shedding mass while disintegrating. Data from other ice cores spanning this time would help determine whether a periodic signal exists. Unfortunately, the GISP2 section is younger and the Vostok core sections older (Brook et al., 2000) than the South Pole core.

At four different times over the course of melting the cores, we wiped down the inside of the funnel with Whatman glass filters and were surprised to find high ^{3}He concentrations and very high ^{3}He/^{4}He ratios in several of these filters. The glass filters themselves have very low ^{3}He blanks (0.0006×10^{-12} cc STP). Two of the filter wipes had ^{3}He concentrations of 3.8×10^{-12} cc STP, one had an extremely high ^{3}He value of 171×10^{-12} cc STP and a ^{3}He/^{4}He of 67×10^{-4}, and one had a moderately high ^{3}He value of 19×10^{-12} cc STP and a ^{3}He/^{4}He of 4×10^{-4} (Appendix D). The filter with the extremely high value had a ^{3}He/^{4}He ratio much higher than that of IDPs and indeed ratios this high have no plausible natural source.

A potential explanation for the ^{3}He on the funnel, and the extraordinarily high ^{3}He/^{4}He ratio, could be the decay of tritium-rich fallout released by nuclear bomb tests. Jouzel et al. (1979) measured tritium concentrations in two South Pole snow pits for the years 1953–1977, allowing us to test this idea. Their data show

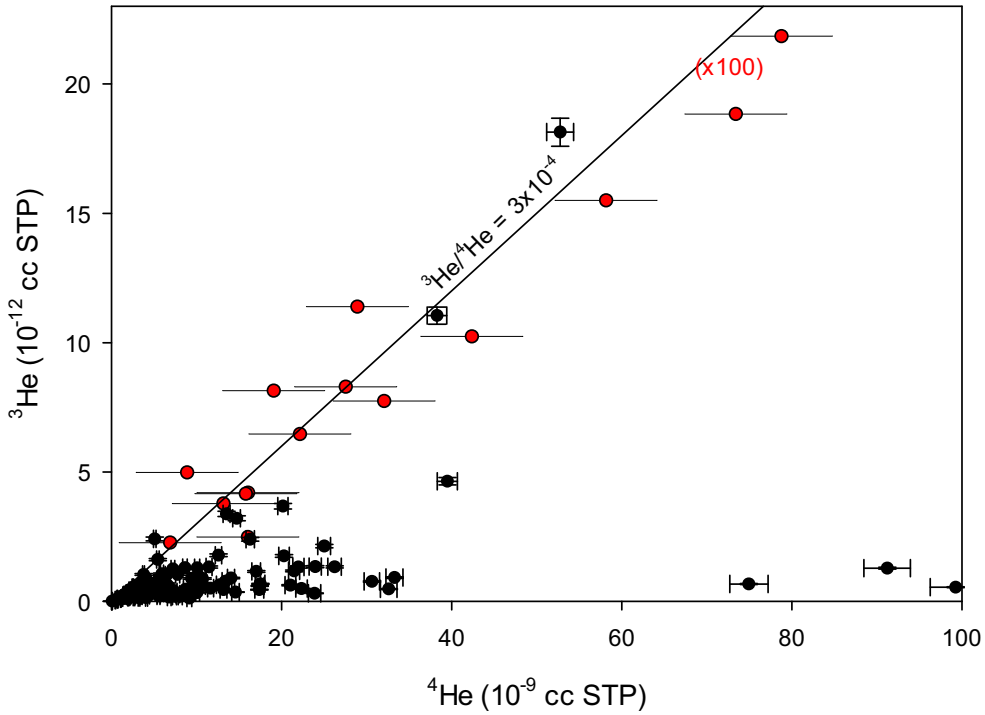

Fig. 9. ^{3}He versus ^{4}He in the 139 cores with measurable ^{4}He are shown with end capped error bars. The two highest ^{3}He values plot along the line of slope ^{3}He/^{4}He = 3.0 × 10^{-4} ratio similar to that defined by the fractionated solar wind in stratospheric IDPs (Nier & Schlutter, 1992). For comparison, we also plot some of the SPA-17 air subsamples ×100 (straight error bars). (Color figure can be viewed at wileyonlinelibrary.com.)

background tritium levels in 1953, a maximum peak in 1966, and above background concentrations in 1977. Only two of the cores we melted could have contained bomb residue, #0 (1978–1981) and #6 (1950–1955). For the years 1953–1955 (core #6), Jouzel et al. (1979) measured five tritium units above background. As they made no measurements for the years 1978–1981 (core #0), we extrapolated the trend in their 1974–1977 data to estimate 20 tritium units for core #0. Combined, 25 units of tritium could have been contained in the cores. Given tritium's half-life of 12.3 yr, all but ~3% would have decayed to ^{3}He by 2018, when we analyzed the samples. We used Jouzel et al.'s (1979) conversion factor of meters of water × Tritium Unit yr^{-1} = 67 × 10^7 atoms of tritium per cm^2 yr^{-1} to calculate ~5 × 10^9 ^{3}He atoms in core #0 and ~1 × 10^9 ^{3}He atoms in core #6. The sum, ~6 × 10^9 atoms, is ~250 × 10^{-12} cc STP of ^{3}He, comparable to the signal we measured from the funnel wipes.

To have been deposited on the funnel, fallout containing ^{3}He must have adhered to the oily residue seen on the melt water surface. This residue coated the funnel interior as the water level dropped during filtering. We do not think this excess ^{3}He adhered to the filters themselves as these had unremarkable ^{3}He concentrations, 0.49 × 10^{-10} cc STP (Core #0) and 0.23 × 10^{-10} cc STP (Core #6) similar to many other core samples. We also do not think the ^{3}He was released off the funnel during melting of the following samples as no systematic increase in ^{3}He values occurred after cores 0 and 6 were melted and no decreases occurred after the funnel cleanings. Still, it is unclear why the ^{3}He would adhere to the oily residue. Previous work has shown that bomb tritium can be organically bound (Eyrolle et al., 2019) but whether organics would host tritium in the biologically poor South Pole environment, and whether organic molecules can retain ^{3}He, are open questions. Note that production of ^{3}He by the beta decay of tritium-rich fallout would not affect the vast majority of the core samples, most of which were deposited before the atomic era.

Comparison of ^{3}He Fluxes We Measured to Those from the Stratosphere and the Geologic Record

One of our goals was to measure the IDP flux in terrestrial surface air. This flux had not been measured and it links the IDP flux measured in the stratosphere with ^{3}He flux measurements made on ice cores and on deep-sea sediments. Figure 11 is a plot of the comparisons.

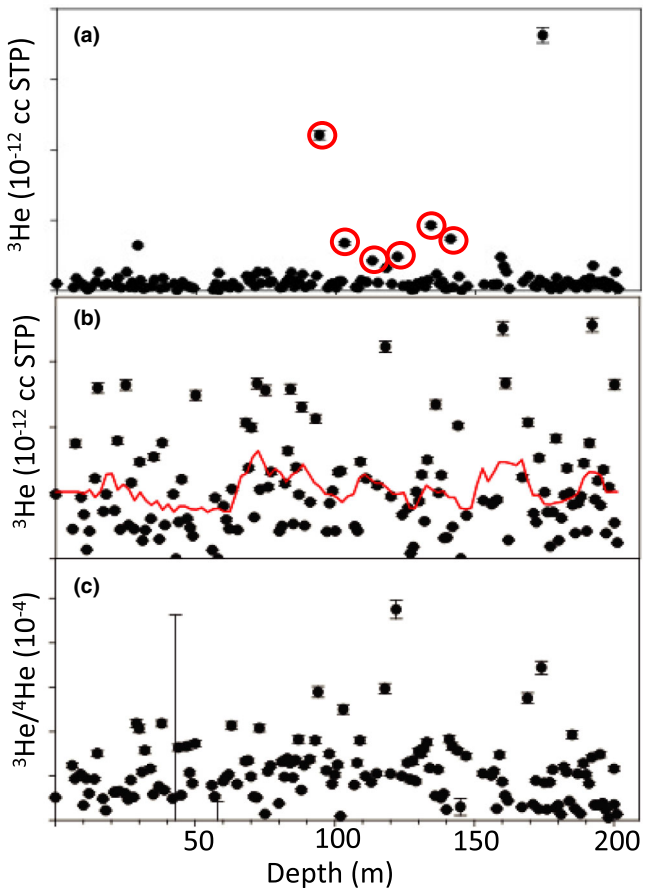

Fig. 10. a) Plot showing ^{3}He concentrations and 1σ error bars for the 139 ice cores with measurable He. Each core sample represents about 10 yr of deposition. The six circled points are outliers that have a reoccurrence interval of 102 ± 20 yr. b) Plot showing ^{3}He concentrations and 1σ error bars for the 130 ice cores with values below 2×10^{-12} cc STP. The squiggly line represents the running average concentration. c) Blank-corrected ^{3}He/^{4}He ratios and 1σ error bars plotted versus ice depth in meters for all the data. (Color figure can be viewed at wileyonlinelibrary.com.)

IDPs were counted on two collection flags flown in the stratosphere and, using the volume of air swept by each flag, yielded IDP concentration per m^3 of air (1.2×10^{-3} m^3 air, Brownlee et al., 1977; 2.5×10^{-3} m^3 air, Zolensky & Mackinnon, 1985). We used these values along with the average ^{3}He concentration measured for IDPs (1.7×10^{-5} cc ^{3}He g^{-1}, Pepin et al., 2000), a settling velocity of 1 cm s^{-1}, an IDP density of 1 g cm^{-3} (Flynn & Sutton, 1991), an average IDP dimension of 10 μm (the average >1000 IDPs collected on flags between January 1982 and September 2017) to calculate the flux of IDPs to the Earth's surface. The two stratospheric IDP concentrations resulted in ^{3}He fluxes of 1.8 and 3.75×10^{-12} cc STP cm^{-2} ka^{-1}, respectively, which we plotted in Fig. 11 as $2.78 \pm 1.4 \times 10^{-12}$ cc STP cm^{-2} ka^{-1}.

For the South Pole air samples, we used the measured ^{3}He concentrations on the filters, the air volume filtered, and the filter area sampled to calculate an average flux for each filter (Table 1). The average ^{3}He flux for all the cm^2 filter subsamples was $0.069 \pm 0.06 \times 10^{-12}$ cc STP cm^{-2}/month or about 83×10^{-11} cc STP cm^{-2} ka^{-1}. The filters, however, had increased deposition rates compared to natural surfaces as the air and entrained particles were suctioned at ~600 times the fall velocity of a 5 μm IDP (600 cm s^{-1} versus 1 cm s^{-1}, Taylor et al., 2020). We corrected for this effect by dividing 83×10^{-11} cc STP cm^{-2} ka^{-1} by 600 resulting in an effective surface flux of $1.4 \pm 1.2 \times 10^{-12}$ cc STP cm^{-2} ka^{-1}.

The 141 South Pole ice core sections had an average ^{3}He value of ~0.5×10^{-12} cc STP. As each core section represented ~10 yr of deposition and the core cross section was 40 cm^2, we calculate a ^{3}He flux of $1.2 \pm 0.3 \times 10^{-12}$ cc STP cm^{-2} ka^{-1}. This value is comparable to the average ^{3}He flux of $0.62 \pm 0.27 \times 10^{-12}$ cc STP cm^{-2} ka^{-1} for the GISP core section and of $0.77 \pm 0.25 \times 10^{-12}$ cc STP cm^{-2} ka^{-1} for the 3.80 ka Vostok section (Brook et al., 2000).

Essentially, the ^{3}He depositional flux measured for the South Pole air filters and ice cores is similar to the stratospheric inputs and the average ^{3}He terrestrial deposition rates measured in sections of the Vostok and GISP2 ice cores and in a variety of deep-sea sediments (Fig. 11). The similarity in fluxes indicates (1) that IDPs carry the ET ^{3}He, which is retained while transiting the atmosphere and during terrestrial burial; (2) poleward stratospheric transport of IDPs must be small or we would see higher ^{3}He fluxes in the ice cores; and (3) that measured mass and particle size distributions of stratospheric IDPs might reasonably be used to assess sedimentary redistribution and the variability in ^{3}He abundances in terrestrial sediments and ice cores. Despite large uncertainties, and the exception of the short-term seasonal fluctuations in the air filter data, variations in ^{3}He flux among sampling localities and archives on the Earth, and over a very large range of time scales, are relatively small.

CONCLUSION

We analyzed ^{3}He abundance in one hundred and eighty 1 cm^2 samples from 13 Antarctic air filters to estimate the ET mass and flux on the filters, assess its heterogeneity, and look for seasonal variations in ^{3}He among the filters. All but two samples contained ET ^{3}He and we calculated an average ^{3}He flux of $1.4 \pm 1.2 \times 10^{-12}$ cc STP cm^{-2} ka^{-1}. The samples are heterogeneous both between filters and among

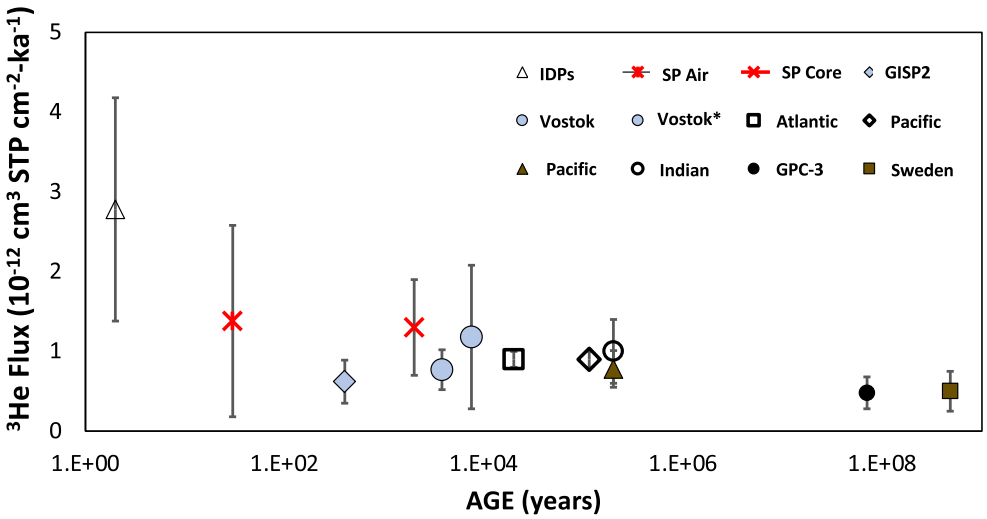

Fig. 11. Average ^{3}He flux and 1σ error bars of values measured from a variety of environments: this work, ✱ South Pole Antarctic air filters and x ice core samples; hollow triangle, two stratospheric IDP values; shaded diamond, Greenland ice core (Brook et al., 2000); shaded circles, Vostok ice core (Brook et al., 2000), shaded circles*, our Vostok estimate using Brook et al. (2000) data. The remaining data were measured on deep-sea sediments: hollow square, Atlantic Ocean cores (Marcantonio et al., 1998); hollow diamond, Pacific Ocean cores (Patterson et al., 1998); filled triangle, and Pacific Ocean cores (Marcantonio et al., 1996); hollow circle, Indian ocean cores (Marcantonio et al., 1999); filled circle, Pacific giant piston core (Farley, 1995) and filled square, marine limestones from Sweden (Patterson et al., 1998). (Color figure can be viewed at wileyonlinelibrary.com.)

Table 2. Data on the nine core samples with ^{3}He concentrations larger than 2×10^{-12} cc STP.

Core depth (m)	29	94	103	113	122	134	141	159	174
^{3}He × 10^{-12} cc STP	3.21	11.05	3.38	2.13	2.41	4.64	3.67	2.40	18.14
^{3}He/^{4}He × 10^{-4}	2.18	2.89	2.50	0.85	4.75	1.17	1.82	1.50	3.44
Depositional decade (AD)*	1790	1170	1080	980	870	740	660	430	250
Time between samples (years)	620	90	100	110	130	80	230	180	

*Calculated from Appendix B.

subsamples from the same filter, consistent with the discrete nature of IDPs, which contain varying amounts of ^{3}He. The data also suggest an annual variation in the ET small particle flux. The Antarctic spring (October and November) has higher ^{3}He values than all other months, possibly from yearly passage through IDP-rich space. The annual mean flux, however, does not differ from that seen in the ice or in the seafloor sediment records.

We analyzed ^{3}He abundance in one hundred and forty-one 1 m-long sections from an ice core drilled at the South Pole in 1981. All but two sections contained ^{3}He and ^{4}He and the helium ratios show that all the ^{3}He is ET with most values below 2×10^{-12} cc STP and nine above that value. As the core was stratigraphically dated and the cross-sectional area known, we calculated an average flux of $1.2 \pm 0.3 \times 10^{-12}$ cc STP cm^{-2} ka^{-1}, ^{3}He values similar to those measured by others on sections of the GISP2 and Vostok ice cores.

The average flux for IDPs as measured by ^{3}He in the South Pole air and ice core samples agrees with flux estimates for IDPs in the stratosphere, and ice and deep-sea sediment cores. This correspondence indicates that IDPs carry the ^{3}He, which is retained during atmospheric transit and terrestrial deposition and burial. Despite large uncertainties, it is striking that variations in ^{3}He flux among sampling localities and archives on the Earth, and over a very large range of time scales, are relatively small.

Acknowledgments—Collection of the South Pole air filters was funded by NASA's Emerging Worlds program 15-EW15-2-009, with added support from NSF's Antarctic Program. We thank NASA and NSF for their support. As authors, we assert no affiliation or involvement in an organization or entity with a financial or nonfinancial interest in the subject matter or materials discussed in this manuscript. We thank Dr.

Hope Ishii and an unknown reviewer for their helpful comments and suggestions.

Data Availability Statement—Data available in article supplementary material.

Editorial Handling—Dr. Donald Brownlee

REFERENCES

Baecker, B., Ott, U., Cordier, C., Folco, L., Trieloff, M., van Ginneken, M., and Rochette, P. 2018. Noble Gases in Micrometeorites from the Transantarctic Mountains. *Geochimica et Cosmochimica Acta* 242: 266–97.

Bodhaine, B. A., Deluisi, J. J., Harris, J. M., Houmere, P., and Bauman, S. 1986. Aerosol Measurements at the South Pole. *Tellus* 33B: 223–35.

Bradley, J. P. 1994. Chemically Anomalous, Pre-Accretionally Irradiated Grains in Interplanetary Dust from Comets. *Science* 265: 925–9.

Bradley, J. P., Brownlee, D. E., and Veblen, D. R. 1983. Pyroxene Whiskers and Platelets in Interplanetary Dust: Evidence of Vapour Phase Growth. *Nature* 301: 473–7.

Brook, E. J., Kurz, M. D., Curtice, J., and Cowburn, S. 2000. Accretion of Interplanetary Dust in Polar Ice. *Geophysical Research Letters* 27: 3145–8.

Brownlee, D. E., Tomandl, D. A., and Olszewski, E. 1977. Interplanetary Dust: A New Source of Extraterrestrial Material for Laboratory Studies. Proceedings, 8th Lunar Science Conference, 149–60.

Busemann, H., Nguyen, A. N., Cody, G. D., Hoppe, P., Kilcoyne, A. L. D., Stroud, R. M., Zega, T. J., and Nittler, L. R. 2009. Ultra-Primitive Interplanetary Dust Particles from the Comet 26P/Grigg-Skjellerup Dust Stream Collection. *Earth and Planetary Science Letters* 288: 44–57.

Cunningham, W. C., and Zoller, W. H. 1981. The Chemical Composition or Remote Area Aerosols. *Journal of Aerosol Science* 12: 367–84.

Dobrica, E., Engrand, C., Duprat, J., Gounelle, M., Leroux, H., Quirico, E., and Rouzaud, J.-N. 2009. Connection Between Micrometeorites and Wild 2 Particles: From Antarctic Snow to Cometary Ices. *Meteoritics & Planetary Science* 44: 1643–61.

Duprat, J., Dobrică, E., Engrand, C., Aléon, J., Marrocchi, Y., Mostefaoui, S., Meibom, A. et al. 2010. Extreme Deuterium Excesses in Ultracarbonaceous Micrometeorites from Central Antarctic Snow. *Science* 328: 742–5.

Eyrolle, F., Copaerd, Y., Lepage, H., Ducros, L., Morereau, A., Grosbois, C., Cassonnet, C., Gurriaran, R., Booth, S., and Desmet, M. 2019. Evidence for Tritium Persistence as Organically Bound Forms in River Sediments Since the Past Nuclear Weapons Tests. *Scientific Report* 9: 11487. https://doi.org/10.1038/s41598-019-47821-1.

Farley, K. A. 1995. Cenozoic Variations in the Flux of Interplanetary Dust Recorded by ^{3}He in a Deep-Sea Sediment. *Nature* 376: 153–6.

Farley, K. A., Love, S. G., and Patterson, D. B. 1997. Atmospheric Entry Heating and Helium Retentivity of Interplanetary Dust Particles. *Geochimica et Cosmochimica Acta* 61: 2309–16.

Farley, K. A., and Patterson, D. B. 1995. A 100-kyr Periodicity in the Flux of Extraterrestrial 3He to the Sea Floor. *Nature* 378: 600–3.

Flynn, G. J., and Sutton, S. R. 1991. Cosmic Dust Particle Densities—Evidence for Two Populations of Stony Micrometeorites. Proceedings, 21st Lunar and Planetary Science Conference, 541.

Hogan, A. W., and Gow, A. J. 1997. Occurrence Frequency of Thickness of Annual Snow Accumulation Layers at South Pole. *Journal of Geophysical Research* 102: 14021–7.

Janches, D., Palo, S. E., Lau, E. M., Avery, S. K., Avery, J. P., de la Pena, S., and Makarov, N. A. 2004. Diurnal and Seasonal Variability of the Meteor Flux at the South Pole Measured with Radars. *Geophysical Research Letters* 31: L20807.

Jenniskens, P., Baggaley, J., Crumpton, I., Aldous, P., Pokorny, P., Janches, D., Gural, P. S. et al. 2017. A Survey of Southern Hemisphere Meteor Showers. *Planetary and Space Science* 154: 1–9.

Jouzel, J., Merlivat, L., Pourchet, M., and Lorius, C. 1979. A Continuous Record of Artificial Tritium Fallout at the South Pole (1954–1978). *Earth and Planetary Science Letters* 45: 188–200.

Kortenkamp, S. J. 2013. Trapping and Dynamical Evolution of Interplanetary Dust Particles in Earth's Quasi-Satellite Resonance. *Icarus* 226: 1550–8.

Kuivinen, K. C., Koci, B. R., Holdsworth, G. W., and Gow, A. J. 1982. South Pole Ice Core Drilling, 1981–1982. *Antarctic Journal of the United States* 17: 89–91.

Love, S. G., and Brownlee, D. E. 1993. A Direct Measurement of the Terrestrial Mass Accretion Rate of Cosmic Dust. *Science* 262: 550–3.

Marcantonio, F., Anderson, R. F., Stute, M., Kumar, N., Schlosser, P., and Mix, A. 1996. Extraterrestrial ^{3}He As a Tracer of Marine Sediment and Transport. *Nature* 383: 705–7.

Marcantonio, F., Higgins, S., Anderson, R. F., Stute, M., Schlosser, P., and Rasbury, E. T. 1998. Terrigeneous Helium in Deep-Sea Sediments. *Geochimica Et Cosmochimica Acta* 62: 1535–43.

Marcantonio, F., Turekian, K. K., Higgins, S., Anderson, R. F., Stute, M., and Schlosser, P. 1999. The Accretion Rate of Extraterrestrial 3He Based on Oceanic 230Th Flux and the Relation to Os Isotope Variation Over the Past 200,000 Years in an Indian Ocean Core. *Earth and Planetary Science Letters* 170: 157–68.

Messenger, S. 2000. Identification of Molecular-Cloud Material in Interplanetary Dust Particles. *Nature* 404: 968–71.

Messenger, S. 2002. Opportunities for the Stratospheric Collection of Dust from Short-Period Comets. *Meteoritics & Planetary Science* 37: 1491–505.

Messenger, S., Keller, L. P., Stadermann, F. J., Walker, R. M., and Zinner, E. 2003. Samples of Stars Beyond the Solar System: Silicate Grains in Interplanetary Dust. *Science* 300: 105–8.

Mosley-Thompson, E., and Thompson, L. 1983. South Pole Ice Core Processing and Microparticle Analysis. *Antarctic Journal of the United States* 18: 118–9.

Nakamura-Messenger, K., Messenger, S., Westphal, A. J., Palma, R. L., and Pepin, R. O. 2015. Mineralogy of Interplanetary Dust Particles from the Comet Giacobini-Zinner Dust Stream Collections (Abstract #5322). 78th Meeting of the Meteoritical Society.

Nier, A. O., and Schlutter, J. D. 1992. Extraction of Helium from Individual Interplanetary Dust Particles by Step-Heating. *Meteoritics* 27: 166–73.

Nier, A. O., and Schlutter, J. D. 2000. Helium and Neon Isotopes in Stratospheric Particles. *Meteoritics* 25: 263–7.

Noguchi, T., Ohashi, N., Tsujimoto, S., Mitsunari, T., Bradley, J. P., Nakamura, T., Toh, S., Stephan, T., Iwata, N., and Imae, N. 2015. Cometary Dust in Antarctic Snow and Ice: Past and Present Chondritic Porous Micrometeorites Preserved on the Earth's Surface. *Earth and Planetary Science Letters* 410: 1–11.

Patterson, D. B., and Farley, K. A. 1998. Extraterrestrial 3He in Seafloor Sediments: Evidence for Correlated 100 kyr Periodicity in the Accretion Rate of Interplanetary Dust, Orbital Parameters, and Quaternary Climate—Orbital Inclination, Not Eccentricity. *Geochimica et Cosmochimica Acta* 62: 3669–82.

Patterson, D. B., Farley, K. A., and Schmitz, B. 1998. Preservation of Extraterrestrial ^{3}He in 480-Ma-old Marine Limestones. *Earth and Planetary Science Letters* 163: 315–25.

Pepin, R. O., Palma, R. L., and Schlutter, D. J. 2000. Noble Gases in Interplanetary Dust Particles, I: The Excess Helium-3 Problem and Estimates of the Relative Fluxes of Solar Wind and Solar Energetic Particles in Interplanetary Space. *Meteoritics & Planetary Science* 35: 495–504.

SUPPORTING INFORMATION

Additional supporting information may be found in the online version of this article.

Appendix A. a) Dedicated building housing the collector; (b) schematic of the collector; (c) schematic of filter assembly (Taylor et al., 2020).

Stauffer, B., and Schwander, J. 1983. Core Processing and Analyses of Ice Cores Drilled at the South Pole. *Antarctic Journal of the United States* 18: 114–6.

Taylor, S., Lever, J. H., Alexander, C. M. O'D., Brownlee, D. E., Messenger, S., Nittler, L. R., Stroud, R. M., Wozniakiewicz, P., and Clemett, S. 2016. Sampling Interplanetary Dust Particles from Antarctic Air. 80th Meeting of the Meteoritical Society.

Taylor, S., Lever, J. H., Burgess, K. D., Stroud, R. M., Brownlee, D. E., Nittler, L. R., Bardyn, A. et al. 2020. Sampling Interplanetary Dust from Antarctic Air. *Meteoritics & Planetary Science* 55: 1–18.

Taylor, S., Lever, J. H., and Harvey, R. P. 2000. Numbers, Types and Compositions of an Unbiased Collection of Cosmic Spherules. *Meteoritics & Planetary Science* 35: 651–66.

Taylor, S., Matrajt, G., and Guan, Y. 2012. Fine-Grained Precursors Dominate the Micrometeorite Flux. *Meteoritics & Planetary Science* 47: 550–64.

Thomas, K. L., Blanford, G. E., Keller, L. P., Klock, W., and McKay, D. S. 1993. Carbon Abundance and Silicate Mineralogy of Anhydrous Interplanetary Dust Particles. *Geochimica et Cosmochimica Acta* 57: 1551–66.

Zolensky, M. E., and Mackinnon, I. D. R. 1985. Accurate Stratospheric Particle Size Distribution from a Flat Plate Collection Surface. *Journal of Geophysical Research* 90: 5801–8.

Appendix B. Stratigraphy of the South Pole core determined by A. Gow.

Appendix C. Blank-corrected helium data for one 1 cm2 air filter subsample.

Appendix D. Data for the 141 core sections melted and analyzed for helium.